Combustion and Flame 161 (2014) 1633–1644

Contents lists available at ScienceDirect

Combustion and Flame

journal homepage: www.elsevier.com/locate/combustflame

Smouldering combustion of peat in wildfires: Inverse modelling of the drying and the thermal and oxidative decomposition kinetics ☆

Xinyan Huang, Guillermo Rein *

Department of Mechanical Engineering, Imperial College London, UK

ARTICLE INFO

Article history:
Received 19 April 2013
Received in revised form 10 December 2013
Accepted 13 December 2013
Available online 23 January 2014

Keywords:
Peat wildfires
Smouldering combustion
Kinetics
Thermogravimetry
Genetic algorithms

ABSTRACT

Smouldering combustion is the driving phenomenon of wildfire in peatlands, like those causing haze episodes in Southeast Asia and Northeast Europe. These are the largest fires on Earth and an extensive source of greenhouse gases, but poorly understood, becoming an emerging research topic in climate-change mitigation. In this work, a series of multistep heterogeneous kinetics are investigated to describe the drying and decomposition in smouldering combustion of peat. The decomposition schemes cover a range of complexity, including 2, 3 or 4-step schemes, and up to 4 solid pseudo-species. The schemes aim to describe the simultaneous pyrolysis and oxidation reactions in smouldering fires. The reaction rates are expressed by Arrhenius law, and a lumped model of mass loss is used to simulate the degradation behaviour seen during thermogravimetric (TG) experiments in both nitrogen and air atmospheres. A genetic algorithm is applied to solve the corresponding inverse problem using TG data from the literature, and find the best kinetic and stoichiometric parameters for four types of boreal peat from different geographical locations (North China, Scotland and Siberia). The results show that at the TG level, all proposed schemes seem to perform well, with a high degree of agreement resulting from the forced optimization in the inverse problem approach. The chemical validity of the schemes is then investigated outside the TG realm and incorporated into a 1-D plug-flow model to study the reaction and the species distribution inside a peat smouldering front. Both lateral and in-depth spread modes are considered. The results show that the drying sub-front is essential, and that the best kinetics is the 4-step decomposition (one pyrolysis, and three oxidations) plus 1-step drying with 5 condensed species (water, peat, α-char, β-char, and ash). This is the first time that the smouldering kinetics and the reaction-zone structure of a peat fire are explained and predicted, thus helping to understand this important natural and widespread phenomenon.

1. Introduction

Smouldering combustion is the slow, low-temperature, flameless burning of porous fuels [1,2] and the most persistent type of combustion phenomena [3]. It is sustained by the heat released when oxygen directly attacks the surface of a solid fuel [1]. It is different from the high-temperature homogenous flaming combustion, but especially common in solid fuels with a tendency to char. Many materials can sustain a smouldering fire, including synthetic fuels such as polyurethane foam or cellulosic insulation, and natural fuels like coal or soils rich in dead organic matter, like peat. Peatlands, made by the natural accumulation of partially decayed vegetation, are the most affected ecosystem by smouldering fires, both in frequency and size. Peat forms organic soil layers of carbon older than 10 thousand years and of depths upon dozens of meters. They are the largest reserves of terrestrial carbon and important ecosystem for a wide range of wildlife habitats, supporting biological diversity, and hydrological integrity [4].

Because of this vast accumulation of natural fuel, once ignited, smouldering peat fires burn for very long periods of time (e.g., months and years) despite extensive rains, weather changes, or fire-fighting attempts. These are the largest fires on Earth and large contributors of greenhouse gases [3,5]. Peat fires occur with some frequency worldwide in tropical, temperate and boreal regions (e.g., Indonesia, Canada, Florida, British Isles, and Siberia). During the 1997 extreme haze event in Southeast Asia, the greenhouse-gas emission from peat fires was equivalent to 13–40% of the global man-made emissions of that year [4]. More recent figures

☆ This is an open-access article distributed under the terms of the Creative Commons Attribution License, which permits unrestricted use, distribution, and reproduction in any medium, provided the original author and source are credited.

* Corresponding author.
E-mail address: G.Rein@imperial.ac.uk (G. Rein).

http://dx.doi.org/10.1016/j.combustflame.2013.12.013
0010-2180/

Nomenclature

A	pre-exponential factor
Da	Damköhler number
E	activation energy
h_0, h_b	original/burning height
L	characteristic thickness of smouldering front
k	heating rate
$m/[m]$	mass fraction (wet basis/dry basis)
$\dot{m}/[\dot{m}]$	mass-loss rate (wet basis/dry basis)
n	reaction order
R	universal gas constant
T	temperature
S	smouldering spread rate
w	weight coefficient
Y_{O_2}	oxygen mass fraction in gas phase

Greeks symbols

α	thermal diffusivity
γ	relative importance in the fitness
δ	thickness of reaction zone
$\dot{\theta}$	non-dimensional reaction rate
ν	stoichiometric coefficient
ξ	non-dimensional spatial location
Π	non-dimensional temperature
ρ	density
τ	characteristic reaction time
Φ	objective function
$\dot{\omega}$	reaction rate

Subscripts

0	initial
α	α-char
αo	α-char oxidation
β	β-char
βo	β-char oxidation
a	ash
cal	calculation
c	char
co	char oxidation
d	in-depth spread
dr	drying
exp	experiment
g	gas phase
i	solid species number
k	reaction number
l	lateral spread
p	peat
pd	peat decomposition
po	peat oxidation
pp	peat pyrolysis
s	solid phase
w	water

estimate that the average emission from peat fires is roughly equivalent to 15% of the man-made emissions [6]. Moreover, the atmospheric release of ancient carbon from the soil and the sensitivity of peat ignition to higher temperatures and drier conditions create a positive feedback mechanism to climate change [3].

For most smouldering fires and under typical conditions, two mechanisms control the rate of spread: the oxygen supply and the heat losses [1]. At the micro scale, smouldering takes place on the surface of a solid fuel, and at the macro scale, it is a bulk phenomenon affecting a porous fuel bed at large. By reacting on the surface of the pores, the fire can penetrate deep into the bed of fuel if oxygen can be transported from a free surface (e.g., open atmosphere, crack or channel). Most peat fires are initiated on the top surface of the fuel bed [3]. The fire then spreads both laterally and in-depth, dominated by forward smouldering (Fig. 1). The lateral spread is enhanced by a direct supply of atmospheric oxygen so its rate is significantly faster than the in-depth spread. It leads to a void in the general shape of an ellipsoid or pan. When the uppermost layer is exposed to wind, the combustion is quenched by heat losses leaving a thin layer of charred material on the very top while smouldering continues just below it. As the fire propagates deeper, a layer of ash also builds up. These two layers, observed often in the field [7], act like an heat insulator to support the reaction front below.

The spread of smouldering fires is dominated by heat and mass transfer processes in a reactive porous media [1,8,9]. Among these mechanisms, the reactivity of peat in the form of a valid and quantified reaction scheme is currently missing. Knowledge of heterogeneous combustion reactions is less developed than homogenous gas-phase kinetics [10,8]. One of the major reasons for this is that it is difficult to experimentally identify the various solid-phase species, especially for a complex organic mixture like peat [11]. Typically, kinetic schemes with just a few global steps and pseudo species are used. Current knowledge shows that smouldering combustion involves simultaneous and competing pyrolysis and oxidation reactions [1,3,9,12]. The endothermic pyrolysis reactions decompose the virgin fuel into pyrolysate gases and char.

Various kinetic schemes of different complexity have been proposed for smouldering combustion. Ohlemiller [1] proposed a 3-step and 3-species scheme, including one pyrolysis and two oxidations, as general scheme for any smoulder-prone fuel. Kashiwagi and Nambu [13] quantified the kinetic parameters of this scheme for cellulose using thermogravimetric analysis (TGA) on small samples (~mg scale) under nitrogen and air atmospheres. Rein et al. [9] studied polyurethane foam, and extended Ohlemiller's scheme to 5-step and 4-species kinetics (two pyrolysis and three oxidations). This extended scheme allows explaining the reaction structure of a smouldering front in both forward and opposed propagation. In doing so, Rein et al. [9] developed a methodology where a genetic algorithm

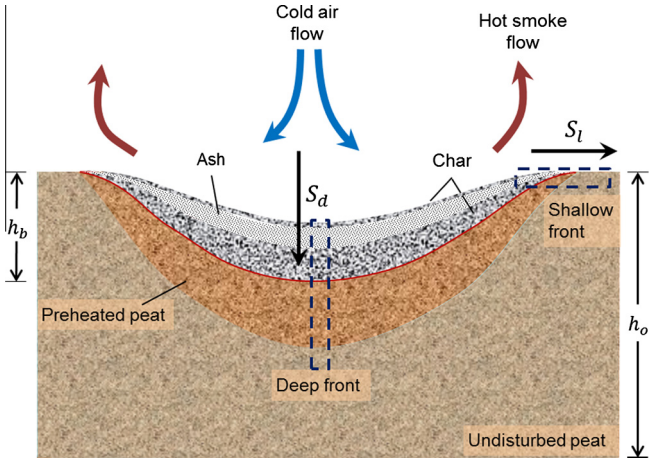

Fig. 1. Schematic diagram of the lateral and in-depth spreads of a smouldering wildfire in a layer of peat.

is used to solve the corresponding inverse problem and find the best sets of kinetic and stoichiometric parameters of the scheme.

Because cellulose is an important component of biological matter, it should serve as foundation for the kinetics of peat. Hadden et al. [12] confirmed that the 3-step and 3-species scheme of Ohlemiller, and Kashiwagi and Nambu [13] qualitatively explained the mass loss measurements taken during peat smouldering of large samples (~100 g). Using TG data from Scottish and Siberian peat samples under air atmospheres, Cancellieri et al. [14] developed a 1-step and 2-species decomposition scheme and calculated analytically the corresponding set of kinetic parameters. Chen et al. [15] proposed and quantified two different schemes for the decomposition of a Chinese boreal peat based on TG data in both nitrogen and air atmospheres. In nitrogen, they proposed a 3-step and 3-species scheme whereas in air they proposed a 2-step and 3-species scheme. But the competition between pyrolysis and oxidation, key to smouldering spread, was not explicitly included or quantified. So far, no completing and quantified kinetic scheme including simultaneous pyrolysis and oxidation reactions has been proposed to explain smouldering peat fires.

In this work, we used TG data from the literature to propose, quantify and investigate a reaction scheme for smouldering of peat based on a 5-step (1-step drying plus 4-step decomposition) and 5-species kinetics scheme. Other simpler 3- and 2-step decomposition schemes are also investigated. Following the work of Rein et al. [9], we employ a genetic algorithm to find the best set of kinetic parameters for each of the schemes and for four different types of peat, from China (CH), Scotland (SC) and Siberia (SI-A and SI-B). The schemes are then applied to simulate the reaction-zone structure using a 1-D steady-state species model. This simple yet comprehensive model allows investigating the effect of the assumed reaction schemes on predicting the front structures in both lateral and in-depth spread modes.

2. Smouldering kinetics of peat

From the viewpoint of fire behaviour, the most important components of peat are the organic matter (OM), water and minerals [16,17]. The left hand side of Fig. 2 shows the relative amounts of the different components found in typical peat samples, although the proportions can vary significantly with the ecosystem type (*i.e.* boreal, temperate or tropical), originating vegetation (e.g., sphagnum or feather) and depth (*i.e.* age and level of decomposition) [18]. Generally, carbon is one of the most abundant chemical elements and its fraction in peat is between 30% and 65% [18], similar to common biomass types [19] and most synthetic polymers [20].

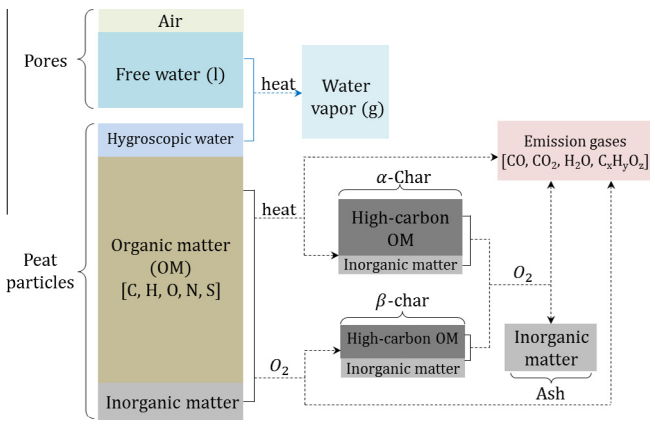

Fig. 2. The composition of peat and a possible decomposition paths and products.

2.1. Moisture content and drying

Peat can hold a wide range of moisture contents (MC[1]) ranging from about 10% under drought conditions to well in excess of 300% under flooded conditions [7]. Thus, the corresponding drying process is crucial in determining the ignition and spread of smouldering peat fires [3,16,17,21]. The prominent role of moisture is such that natural or anthropogenic-induced droughts are the leading cause of smouldering megafires [3].

Condensed-phase water can exist within a porous media like peat in two different forms: hygroscopic (<10 vol% or MC < 100%) and free (capillary and gravity, 10–40 vol%) [22] (see Fig. 2). The drying of peat is a multi-step physicochemical process that takes place at relatively low temperatures while the thermal decomposition is negligible. At high MC, water evaporation from porous media starts with the gravity free water in the large pores and then the capillary water in the small pores. As the water content decreases, the drying process finishes with the evaporation of the hygroscopic water bonded to the surface of peat particles [22]. Experimental studies [16,17,21] show that peat is not susceptible to fire ignition when the MC is above 115%. Therefore, the drying of free water is of low interest in peat fires and not studied in this work. Hygroscopic water in porous media is dominant at MC < 100% and can exist above the boiling temperature. In this form, the water is bonded to the solid surface within a thin film of 4–5 molecules thickness, so it cannot flow but only change to the vapour phase as temperature increases [23]. This allows modelling the drying as the dissociation step of peat-bound water as follows:

$$\text{Peat} \cdot \nu_w H_2O \rightarrow \text{Peat} + \nu_w \text{H}_2\text{O}(g), \quad \text{(Drying)} \tag{1}$$

where ν_w = MC is the initial moisture content in the dry basis, and the dot in Eq. (1) means the water is bonded to the peat. The conversion of the mass fraction from dry basis ($[m_i]$) to the wet basis (m_i) is $m_i = [m_i](1 - m_{w,0}) = [m_i]/(1 + \text{MC})$. This drying step is mainly a chemical process, and can be modelled with a 1-step Arrhenius expression [24,25].

2.2. Peat decomposition

As temperature increases, the decomposition of the organic soil becomes dominant. Despite of the complex composition and chemical process, experimental observations [12,14,15,21] suggest that a few steps of global reactions can capture the most important behaviour of the thermal and oxidative degradation of peat. TG experiments (to be presented later) in nitrogen atmosphere give information on the thermal decomposition and show that there is at least a 1-step pyrolysis process. Results in air atmosphere provide information on the simultaneous thermal and oxidative decomposition, and show (to be presented later) that at least two additional steps are needed.

The validity and accuracy of a proposed kinetic scheme reflects the understanding of the chemical process and the quantity and quality of the available experimental data, but little is known about the decomposition of peat. Further referring to the decomposition of biomasses [26,27] and cellulose [13] and taking into account that smouldering involves the competition of pyrolysis and heterogeneous oxidations [3,12], we propose here that the most complete yet simple global decomposition scheme for peat would be a 4-step, including peat pyrolysis, peat oxidation, β-char oxidation, and α-char oxidation with 4 solid pseudo-species (peat, α-char, β-char, and ash):

[1] Moisture content (MC) is defined in dry basis as the mass of water divided by the mass of a dried soil sample. The conversion from volume % is made assuming a sample density of 110 kg/m^3, typical for peat [16].

$$\text{Peat} \rightarrow \nu_{\alpha,pp}\alpha - \text{Char} + \nu_{g,pp}\text{Gas}, \quad \text{(Peat Pyrol.)} \tag{2}$$

$$\text{Peat} + \nu_{O_2,po}O_2 \rightarrow \nu_{\beta,po}\beta - \text{Char} + \nu_{g,po}\text{Gas}, \quad \text{(Peat Oxid.)} \tag{3}$$

$$\beta - \text{Char} + \nu_{O_2,\beta o}O_2 \rightarrow \nu_{a,\beta o}\text{Ash} + \nu_{g,\beta o}\text{Gas}, \quad (\beta - \text{Char Oxid.}) \tag{4}$$

$$\alpha - \text{Char} + \nu_{O_2,\alpha o}O_2 \rightarrow \nu_{a,\alpha o}\text{Ash} + \nu_{g,\alpha o}\text{Gas}, \quad (\alpha - \text{Char Oxid.}) \tag{5}$$

where $\nu_{i,k}$ is the mass stoichiometric coefficient of species i $(= O_2, g, p, \alpha, \beta, a)$ in the reaction k $(= pp, po, \beta o, \alpha o)$. This scheme is also conceptually represented in Fig. 2. Overall, there are two possible parallel paths involved: (a) peat→ α-char →ash (Eqs. (2) and (5)), and (b) peat→ β-char →ash (Eqs. (3) and (4)).

Char is also called pyrogenic char or black carbon, and contains carbon in a porous structure but also other hydrocarbons and mineral species [11]. Due to the release of gaseous OM (e.g., volatiles and pyrolysate) in Eqs. (2) or (3), char has a lower organic content (OC) than the original peat (see Fig. 2). The α-char and β-char are yielded through different decomposing mechanisms, so in general they have different structures, compositions, and reactivities. The peak temperature in smouldering combustion of peat is about 800 K [12,21], so the high-temperature pyrolysis of char and the decomposition of the minerals [15] are negligible and not included in the kinetics.

2.3. Reaction rate and mass evolution in TG experiment

Arrhenius law remains the best expression to quantify and to simulate condensed-phase reactions [10,9]. The reaction rate for each of the reactions in Eqs. (1)–(5) is as follows:

$$\dot{\omega}_k(T, m_i, Y_{O_2}) = (m_{i,\Sigma})A_k e^{-E_k/RT}\left(\frac{m_i}{m_{i,\Sigma}}\right)^{n_k} Y_{O_2}^{n_{O_2,k}} \tag{6}$$

where kinetic parameters A_k, E_k, n_k and $n_{O_2,k}$ are the pre-exponential factor, activation energy, reaction-order of condensed species, and reaction-order of oxygen in the reaction k, respectively. The mass fraction of condensed species i, m_i, respects to the initial sample mass (*i.e.* in the wet basis). The cumulative mass is defined as $m_{i,\Sigma} = m_{i,0} + \int_0^t \dot{\omega}_{fi} d\tau$, which remains constant or increases monotonically [28]. During the drying stage, the mass loss of the OM in peat is assumed to be negligible and that it does not interfere with the drying process. This is confirmed in the later sections of this work.

For each reaction, the kinetic and stoichiometric ($\nu_{i,k}$) parameters for peat are unknown, and difficult to be measured directly. TG experiments provide an ideal environment of controllable atmosphere and heating rate, and negligible thermal gradient and transport effects during the degradation of the small solid samples (~mg). Therefore, the mass-loss rate measured during TG can be well simulated by a lumped model, which for the 5-step kinetics above is as follows:

$$\begin{aligned}
\dot{m}_w &= -\dot{\omega}_{dr},\\
\dot{m}_p &= -\dot{\omega}_{pp} - \dot{\omega}_{po},\\
\dot{m}_\beta &= \nu_{\beta,po}\dot{\omega}_{po} - \dot{\omega}_{\beta o},\\
\dot{m}_\alpha &= \nu_{\alpha,pp}\dot{\omega}_{pp} - \dot{\omega}_{\alpha o},\\
\dot{m}_a &= \nu_{a,\beta o}\dot{\omega}_{\beta o} + \nu_{a,\alpha o}\dot{\omega}_{\alpha o}.
\end{aligned} \tag{7}$$

Thus, the total mass-loss rate of the sample is

$$\begin{aligned}
\dot{m} &= \dot{m}_w + \dot{m}_p + \dot{m}_\beta + \dot{m}_\alpha + \dot{m}_a\\
&= -\dot{\omega}_{dr} + (\nu_{\alpha,pp} - 1)\dot{\omega}_{pp} + (\nu_{\beta,po} - 1)\dot{\omega}_{po} + (\nu_{a,\beta o} - 1)\dot{\omega}_{\beta o}\\
&\quad + (\nu_{a,\alpha o} - 1)\dot{\omega}_{\alpha o}.
\end{aligned} \tag{8}$$

The initial conditions, rate of temperature increase, and atmosphere oxygen fraction are set to simulate the environment in the corresponding TG experiment as follows,

$$\begin{cases}
m_w(0) = m_{w,0},\\
m_p(0) = 1 - m_{w,0},\\
m_\alpha(0) = m_\beta(0) = m_a(0) = 0,\\
T(0) = T_0,
\end{cases} \tag{9}$$

$$\begin{cases}
Y_{O_2} = 0(N_2) \text{ or } Y_{O_2} = 0.232(\text{air}),\\
\frac{dT}{dt} = k,
\end{cases} \tag{10}$$

where the wet-basis moisture content ($m_{w,0}$) can be converted to the dry-basis as $\text{MC} = m_{w,0}/(1 - m_{w,0})$; k is the heating-rate constant, *i.e.* the controlled temperature-increase rate inside the oven, converting the time-dependent problem into a temperature-dependent problem. Then, unknown parameters can be inversely modelled by matching the simulated mass losses with those in TG experiments.

TG data at various oxygen concentrations is needed to find the reaction-order for oxygen ($n_{O_2,k}$). As a first approximation, that $n_{O_2,k} = 1$ in oxidation and $n_{O_2,k} = 0$ in pyrolysis (*i.e.* oxygen independent) is assumed [9]. If a TG test is only preformed in air (e.g., [14]), the scheme cannot distinguish the pyrolysis from the peat oxidation, and the accurate value for $n_{O_2,k}$ cannot be found.

Because the mass of inorganic matter (or minerals) is conserved during smouldering and becomes the ash after combustion (see Fig. 2), the stoichiometric parameters in consecutive reactions satisfy

$$\text{IC} = 1 - \text{OC} = \nu_{\alpha,pp}\nu_{a,\alpha o} = \nu_{\beta,po}\nu_{a,\beta o}, \tag{11}$$

where the initial inorganic content (IC) of peat relates to the initial MC and the mass of ash after combustion (m_a), as $\text{IC} = m_a/(1 - m_{w,0}) = m_a(1 + \text{MC})$.

Therefore, this system of ordinary differential equations contains a total of 18 unknown parameters: (A_k, E_k, n_k) from the 5 reactions in the form of Eq. (6), plus $m_{w,0}, \nu_{\alpha,pp}$ and $\nu_{\beta,po}$. The large number of unknowns produces a large search space and results in a complex landscape for the optimization, with numerous local maxima and minima. Solving it demands an efficient multi-dimensional optimization algorithm such as a Genetic Algorithm (GA) which has been used successfully in previous related work [9].

3. Inverse kinetics modelling

3.1. Genetic algorithm and optimization techniques

A Genetic Algorithm (GA) is a heuristic search method, imitating the principles of biological adaption based on Darwinian survival-of-the-fittest theory [29,30]. In a GA, the candidate solutions represent the individuals in a population that evolves with time in a predetermined environment. It has been widely used in research of combustion science, such as engine design [31], gas kinetics [32,33], condensed-phase kinetics [9], and fire pyrolysis [34].

The search goal is to achieve a minimum error with experimental TG data, defined as:

$$\Phi_i = \gamma\frac{\sum |\dot{m}_{cal,i} - \dot{m}_{exp,i}|}{\sum \dot{m}_{exp,i}} + (1 - \gamma)\frac{\sum |m_{cal,i} - m_{exp,i}|}{\sum m_{exp,i}}, \tag{12}$$

which accounts for relative errors in both the total mass (m) and the mass-loss rate ($\dot{m}$), and γ is set to 0.5, giving equal importance to each term. The summations in Eq. (12) are evaluated for each experiment data in the temperature range (from 300 to 900 K). In order to improve the uniqueness of solution, TG tests conducted in different atmospheres and heating rates can be optimized simultaneously. Then, we define the overall error as the linear combination of the error in each test as

$$\Phi = \sum_{i=1}^{N} w_i \Phi_i, \qquad \left(\sum_{i=1}^{N} w_i = 1 \right), \tag{13}$$

where w_i is the weight coefficient. The GA code used here is GAOT [35]. Generally, good results are reached with a population size between 100 and 500. The algorithm is stopped when no further decrease in Φ occurs after several hundred generations. Typically, convergence was achieved in less than 500 generations, requiring a total computer time of about 2 h with an Intel *i*7-3770 (3.40 GHz × 8) CPU.

3.2. Kinetic parameters of CH peat

We first determine the kinetic and stoichiometric parameters for an air-dried low-carbon Chinese (CH) peat (see Table 1). The TG experiments were conducted by Chen et al. [15] at three heating rates, k = 7.5, 10, and 12.5 K/min, in both nitrogen (Fig. 3), and air atmospheres (Fig. 4). All six tests are modelled simultaneously with a same weight coefficient ($w_i = 1/6$). The best value found for each parameter is listed in Table 2, together with the range of values of other good solutions (*i.e.* top individuals satisfying $\Delta\Phi = \Phi - \Phi_{min} < 0.3\%$). The experimental and simulated TG curves are compared in Figs. 3 (nitrogen) and 4 (air).

In general, the proposed kinetics captures the position and magnitude of all TG data. The minimum value of the error is $\Phi_{min} = 7.4\%$. The best value found for the initial moisture content, MC = 8.4% is similar to the value of 9% found independently in [15] for the same peat sample. In nitrogen experiments (Fig. 3b), scrutiny reveals that the third (soft) peak in mass-loss rate just above 600 K cannot be simulated by the 1-step pyrolysis of Eq. (2). However, this second peak is of low intensity, taking place very close to the first higher peak between 580 and 620 K. Moreover, as it would

Table 1
Characteristics of four peat samples.

Name	Location	Peat type	Decomposition degree	Organic content (OC[a])	Carbon fraction
CH [15]	North China	Coniferous forest	Undecomposed [18]	Low (81.7%)	Low (~ 30%)
SC [14]	Scotland (Sco-1)	High moor	42%	High (98.2%)	High (53.32%)
SI-A [14]	Siberia (Sib-2)	High moor	20%	High (97.6%)	Medium (44.81%)
SI-B [14]	Siberia (Sib-3)	Transition moor	10.5%	Medium (87.9%)	Medium (43.09%)

[a] Estimated from this study (dry basis).

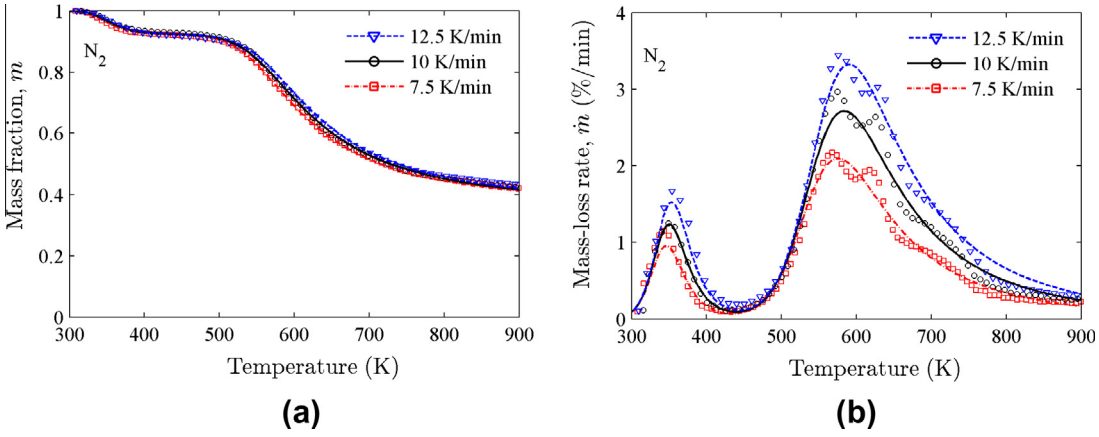

Fig. 3. (a) mass, and (b) mass-loss rate of CH peat in nitrogen (wet basis) as a function of temperature for three heating rates. Marks: experimental data [15], and lines: simulations.

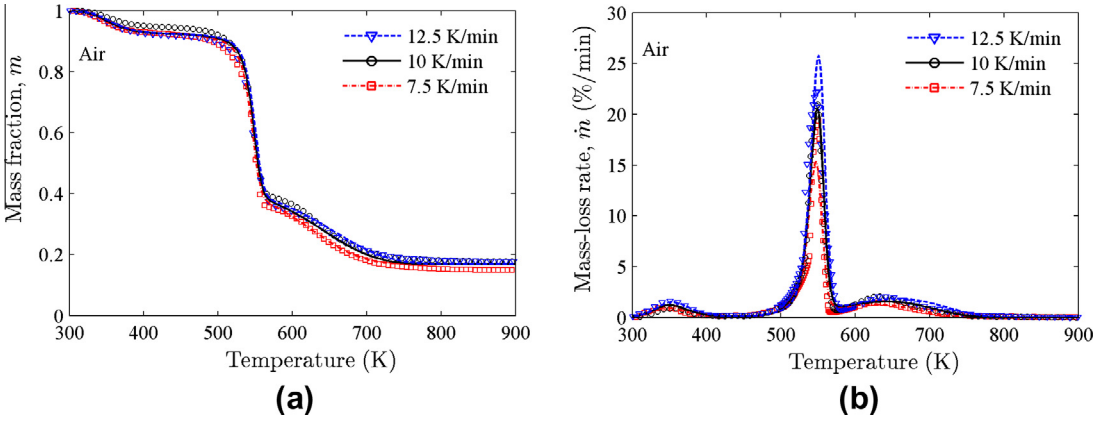

Fig. 4. (a) mass, and (b) mass-loss rate of CH peat in air (wet basis) as a function of temperature for three heating rates. Marks: experimental data [15], and lines: simulations. Note that the scale in Fig. 4b is different from that in Figs. 3b.

Table 2
Kinetic and stoichiometric parameters for the CH peat sample with the 5-step scheme.

Parameter	Best	Range	Unit
MC	8.4	[8.2, 9.3]	(%)
OC	81.7	–	(%)
$\lg A_{dr}$	8.12	[6.05, 8.65]	$\lg(s^{-1})$
E_{dr}	67.8	[54.8, 71.3]	kJ/mol
n_{dr}	2.37	[1.77, 2.77]	–
$\lg A_{pp}$	5.28	[4.28, 5.77]	$\lg(s^{-1})$
E_{pp}	86.0	[75.9, 91.1]	kJ/mol
n_{pp}	4.44	[3.58, 4.47]	–
$\nu_{\alpha,pp}$	0.39	[0.39, 0.43]	kg/kg
$\lg A_{po}$	30.6	[28.3, 34.5]	$\lg(s^{-1})$
E_{po}	332	[309, 373]	kJ/mol
n_{po}	1.36	[1.24, 1.67]	–
$\nu_{\beta,po}$	0.43	[0.42, 0.45]	kg/kg
$\lg A_{\beta o}$	1.86	[1.68, 2.19]	$\lg(s^{-1})$
$E_{\beta o}$	46.9	[45.0, 51.0]	kJ/mol
$n_{\beta o}$	0.93	[0.85, 0.93]	–
$\nu_{a,\beta o}$ [a]	0.43	–	kg/kg
$\lg A_{\alpha o}$	2.57	[1.95, 2.57]	$\lg(s^{-1})$
$E_{\alpha o}$	54.1	[54.1, 60.4]	kJ/mol
$n_{\alpha o}$	1.53	[0.96, 1.57]	–
$\nu_{a,\alpha o}$ [a]	0.47	–	kg/kg
Φ	7.4	< 7.7	(%)

[a] Calculated from Eq. (11).

be seen in Fig. 4b, above 550 K, the oxidation of peat or char is already dominant, and pyrolysis does not play an important role.

The simulated reaction rates, $\dot{\omega}_i$, and the dry-basis mass fractions, $[m_i]$, at $k = 10$ K/min are shown in Fig. 5. The first peak of mass-loss rate in both nitrogen (Fig. 3b) and air (Figs. 4b) between 300 and 400 K, is correctly simulated by Eq. (1) as the drying stage. In nitrogen (Fig. 3b), the subsequent peak is simulated by Eq. (2) as the peat pyrolysis. No clear overlapping between drying and pyrolysis is observed, which confirms the assumption of negligible peat decomposition during drying. In air (Fig. 5b), after drying, the simultaneous pyrolysis and oxidation reactions of peat as well as the subsequent β-char oxidation overlap in a narrow temperature range (500–570 K), producing the highest peak of mass-loss rate in Fig. 4b. Comparison between nitrogen and air simulations shows that in TG, oxidations dominate the peat decomposition ($\dot{\omega}_{po}^{max}/\dot{\omega}_{pp}^{max} = 19$). Figure 5d shows that the production of β-char is larger than that of α-char ($m_{\beta}^{max}/m_{\alpha}^{max} = 11$). This also explains that above 500 K the oxidation rate of β-char is larger than that of α-char ($\dot{\omega}_{\beta o}^{max}/\dot{\omega}_{\alpha o}^{max} = 12$ in Fig. 5b). In other words, for this sample and under TG conditions, the reaction path (b) (Peat→ β-char →ash) is about one order of magnitude faster than the alternative path (a) (Peat→ α-char →ash).

In Table 2, the best values found for the kinetic triplet (A_k, E_k, and n_k) fall in relatively wide ranges. However, their wide variations yield small differences in terms of error ($\Delta\Phi < 0.3\%$). Investigation of interdependence inside these ranges shows a clear linear compensation effect [10,36] between $\lg A_k$ and E_k. The sample data is plotted in Fig. 6a and fitted as

$$\begin{cases} \lg A_{dr} = -2.52 + 0.157E_{dr}, & (R_{dr}^2 = 1.00) \\ \lg A_{pp} = -3.21 + 0.099E_{pp}, & (R_{pp}^2 = 1.00) \\ \lg A_{po} = -1.58 + 0.097E_{po}, & (R_{po}^2 = 1.00) \\ \lg A_{\beta o} = -2.26 + 0.087E_{\beta o}, & (R_{\beta o}^2 = 0.99) \\ \lg A_{\alpha o} = 4.30 - 0.038E_{\alpha o}, & (R_{\alpha o}^2 = 0.44) \end{cases} \quad (14)$$

showing a high linearity as measured by the R^2 coefficient, except for the α-char oxidation. The reaction order, n_k, also depends on E_k for all reactions (see Fig. 6b). Except for $n_{\alpha o}$, all other n_k increases linearly with E_k, although the scatter of data is significant. Therefore, the kinetic triplet (A_k, E_k, and n_k) are interdependent, as mathematically proved for TG conditions by [37]. For α-char oxidation, the most likely reason for the non-linear dependence of the triplet is that its very low reaction rate carries a low contribution to the total mass loss measured in TG. This is a limitation in the experimental data available that cannot provide sufficiently information to fix the temperature range and reaction rate of α-char oxidation accurately. Therefore, this serves as evidence that adding more reaction steps would not improve the interpretation of this TG data.

Finding the right level of complexity is a key question in kinetics modelling. In order to explore this issue, a reduced 3-step

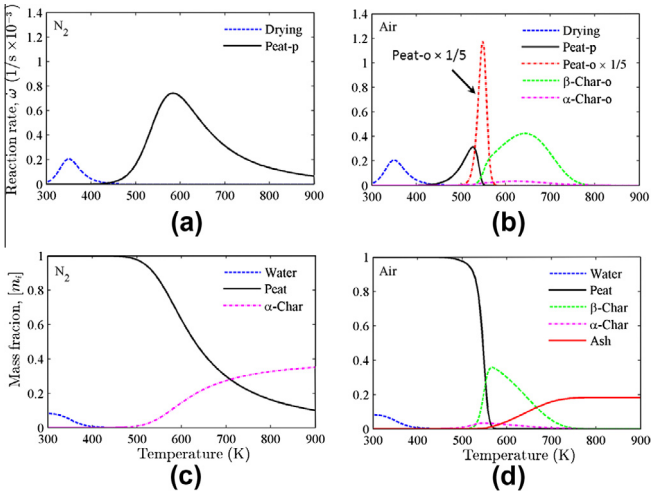

Fig. 5. Simulation results of the TG experiment for CH peat at $k = 10$ K/min, (a) reaction rates, $\dot{\omega}_k$, and (b) dry-basis mass fractions, $[m_i]$, in nitrogen; (c) reaction rates, $\dot{\omega}_i$, and (d) dry-basis mass fractions, $[m_i]$, in air. The rate of peat oxidation is scaled down by 1/5 due to its exceptionally high peak.

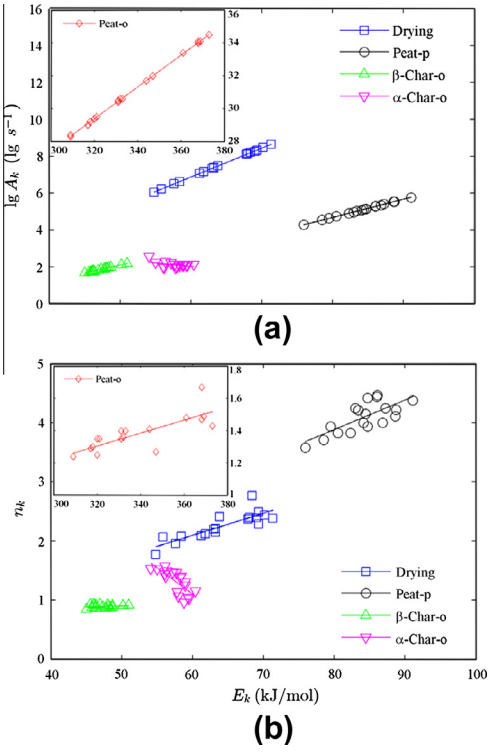

Fig. 6. Interdependence among the kinetic parameters: (a) $\lg(A_k)$ against E_k, and (b) n_k against E_k; data from good solutions satisfying $\Delta\Phi < 0.1\%$. The inserted subfigures have different scales.

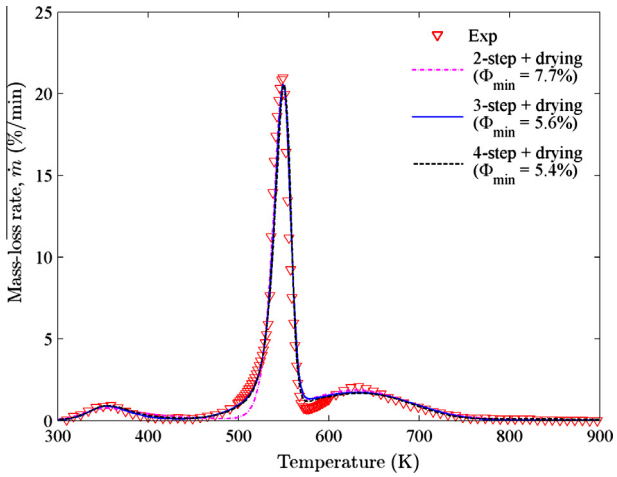

Fig. 7. Mass-loss rate of CH peat in air ($k = 10$ K/min) simulated by chemical schemes with different number of steps. The number of steps in the legend includes the drying plus the peat decomposition steps.

decomposition scheme with 3 solid pseudo-species for peat decomposition is obtained,

$$\begin{aligned} &\text{Peat} \rightarrow \nu_{\alpha,pp}\text{Char} + \nu_{g,pp}\text{Gas}, \quad \text{(Peat Pyrol.)} \\ &\text{Peat} + \nu_{O_2,po}O_2 \rightarrow \nu_{c,po}\text{Char} + \nu_{g,po}\text{Gas}, \quad \text{(Peat Oxid.)} \\ &\text{Char} + \nu_{O_2,co}O_2 \rightarrow \nu_{a,co}\text{Ash} + \nu_{g,co}\text{Gas}, \quad \text{(Char Oxid.)} \end{aligned} \tag{15}$$

where only one type of char is considered. Chen et al. [15] proposed a more reduced 2-step scheme with 3 solid pseudo-species by neglecting the peat pyrolysis of Eq. (2) and lumping it into the peat oxidation of Eq. (3),

$$\begin{aligned} &\text{Peat} + \nu_{O_2,po}O_2 \rightarrow \nu_{c,po}\text{Char} + \nu_{g,po}\text{Gas}, \quad \text{(Peat Oxid.)} \\ &\text{Char} + \nu_{O_2,co}O_2 \rightarrow \nu_{a,co}\text{Ash} + \nu_{g,co}\text{Gas}. \quad \text{(Char Oxid.)} \end{aligned} \tag{16}$$

Figure 7 compares the results obtained with the different decomposition schemes plus drying, where only the mass-loss rate in air at 10 K/min is considered for the optimization and reported. No clear difference can be found between different schemes, and their degrees of fit are very similar: $\Phi_{min} = 7.7\%$ (2-step), 5.6% (3-step), and 5.4% (4-step). One major reason for such a good fit is that under TG conditions and air atmosphere, the reaction path (b) (Peat $\rightarrow\beta$-char $\rightarrow$ash) overwhelms the parallel path (a) (Peat $\rightarrow\alpha$-char $\rightarrow$ash) so giving less importance to some of the reactions in the 4-step decomposition.

As the results show here, it is difficult to discern the relatively superiority of each schemes in the TG realm because the inverse modelling approach forces good results in all cases. However, in Section 4, we settle this issue by applying these schemes and the kinetics parameters into a plug-flow model of a smouldering front.

3.3. Kinetic parameters of carbon-rich peat

The kinetic and stoichiometric parameters for another three oven-dried carbon-rich peat from Scotland (SC) and Siberia (SI-A and SI-B) have been found. The characteristics of the samples are listed in Table 1. The TG experiments were conducted by Cancellieri et al. [14] at three heating rates, $k = 10$, 20, and 30 K/min, in air only. The TG data is available at 500–900 K, so the drying process cannot be explored. Note that without TG results in a non-oxidizing atmosphere (e.g., nitrogen), the separation between the pyrolysis and oxidations reactions cannot be established thus leading to inaccuracies in the kinetics.

The highest heating rate of 30 K/min of this TG data is close to range of heating rates observed experimentally in smouldering peat samples (between 30 and 50 K/min [38]). For this group of experimental data, the quality of inversely modelled kinetic parameters is investigated by optimizing with only the 20 K/min data, and using the other two heating rates (10 and 30 K/min) as blind predictions.

Due to the interdependence among three kinetics parameters, all reaction orders ($n_k = 1$) for the SI-A peat are fixed here. The values found for all kinetic and stoichiometric parameters are listed in Table 3. The minimum errors are $\Phi_{min} = 1.5\%$ (SC), 4.5% (SI-A), and 3.5% (SI-B). The experimental and simulated TG curves are compared in Fig. 8. In general, the proposed kinetics successfully captures the position and magnitude of all TG curves between 500 and 900 K at 20 K/min. The blind predictions for 10 and 30 K/min also show a good agreement, demonstrating the capabilities of the kinetic scheme when extrapolated to different heating rates. A strong linear compensation effect among $\lg A_k$ and E_k is also observed for all reactions of 3 peat, similarly to the CH peat in Fig. 6.

Table 3
Kinetic and stoichiometric parameters for Scottish and Siberian peat samples with the 4-step scheme of peat decomposition.

Parameter	Peat type						Unit
	SC		SI-A		SI-B		
	Best	Range	Best	Range	Best	Range	
MC	8.1	[8.0, 8.2]	11.3	[11.2, 11.5]	8.8	[8.7, 8.9]	(%)
OC	98.2	–	97.6	–	87.9	–	(%)
$\lg A_{pp}$	5.92	[5.75, 6.31]	4.81	[4.79, 5.99]	4.63	[3.58, 5.66]	$\lg(s^{-1})$
E_{pp}	93.3	[91.1, 97.6]	80.0	[80.0, 93.5]	74.3	[63.0, 84.6]	kJ/mol
n_{pp}	1.01	[0.96, 1.05]	1	–	1.64	[1.53, 1.91]	–
$\nu_{\alpha,pp}$	0.75	[0.70, 0.97]	0.55	[0.55, 0.68]	0.93	[0.92, 0.99]	kg/kg
$\lg A_{po}$	6.51	[5.92, 6.69]	5.72	[4.26, 5.72]	7.62	[6.82, 8.80]	$\lg(s^{-1})$
E_{po}	89.8	[83.7, 91.6]	85.1	[68.4, 85.1]	104	[94.6, 116]	kJ/mol
n_{po}	1.03	[0.91, 1.03]	1	–	0.65	[0.63, 0.80]	–
$\nu_{\beta,po}$	0.65	[0.53, 0.68]	0.46	[0.35, 0.46]	0.30	[0.26, 0.32]	kg/kg
$\lg A_{\beta o}$	1.65	[1.61, 1.73]	50.3	[49.6, 63.8]	5.06	[5.06, 5.83]	$\lg(s^{-1})$
$E_{\beta o}$	52.4	[51.8, 53.7]	689	[680, 872]	91.7	[91.7, 112]	kJ/mol
$n_{\beta o}$	0.54	[0.48, 0.57]	1	–	0.59	[0.50,0.63]	–
$\nu_{a,\beta o}$[a]	0.03	–	0.05	–	0.40	–	kg/kg
$\lg A_{\alpha o}$	7.04	[6.63, 7.75]	2.83	[2.16, 3.56]	4.69	[3.93, 4.91]	$\lg(s^{-1})$
$E_{\alpha o}$	112	[106, 120]	59.8	[51.0, 69.3]	80.8	[71.5, 83.4]	kJ/mol
$n_{\alpha o}$	1.85	[1.79, 2.14]	1	–	1.49	[1.34, 1.55]	–
$\nu_{a,\alpha o}$[a]	0.02	–	0.04	–	0.13	–	kg/kg
Φ	1.5	<1.7	4.5	<4.8	3.5	<3.7	(%)

[a] Calculated from Eq. (11).

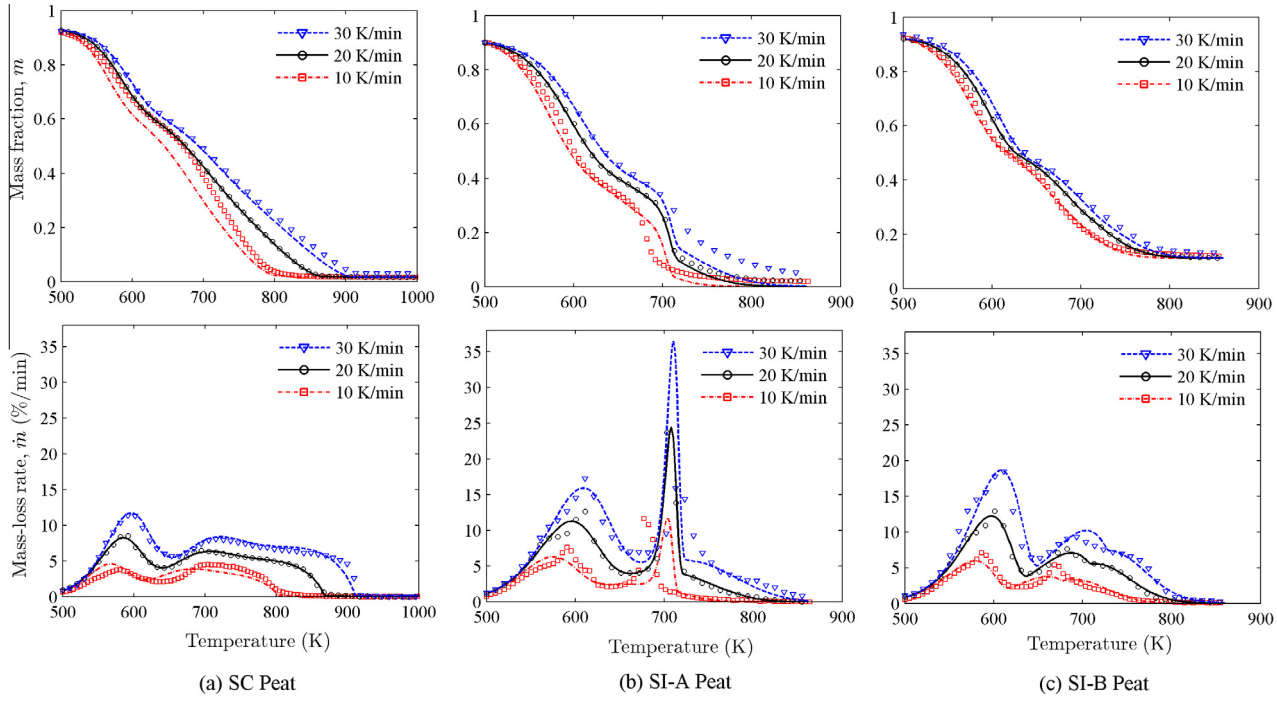

Fig. 8. The wet-basis mass loss (up) and mass-loss rate (down) of (a) SC, (b) SI-A, and (c) SI-B samples in air for three heating rates. Marks: experimental data [14], and lines: simulations.

The simulated reaction rates, $\dot{\omega}_k$, and the dry-basis mass fractions, m_i, at 20 K/min are explored in Fig. 9. Similar to the results of CH samples, the rates of peat pyrolysis and oxidation peak at 550–600 K, and then rates of two char oxidations peak at about 700 K. But unlike the CH sample which has a large peat-oxidation rate and a small char-oxidation rate, these high-OC samples show that the maximum value of all reactions rates are in the same order of magnitude. Also, α-char and β-char oxidations play a similarly important role at high temperature. These suggest that the differences in reactivity seen between CH and SC/SI samples are due to the different carbon contents and decomposition degrees.

The influence of the number of reactions is also discussed here. Figure 10 compares the original 4-step decomposition scheme in Eqs. (2)–(5) with the 3-step scheme in Eq. (15) and the 2-step scheme in Eq. (16) by modelling the mass-loss rate at 20 K/min. Both the 3-step and 2-step schemes can roughly capture the two peaks of mass-loss rate, but the agreement is poor, especially for high-moor SC and SI-A peat. The difference in the degree of fit between 2-step and 3-step schemes is very tiny (difficult to discriminate for SC and SI-A samples in Fig. 10). Moreover, the simulation also reveals that with 3-step or 2-step kinetics the disagreement further increases in the blind prediction of other heating rates.

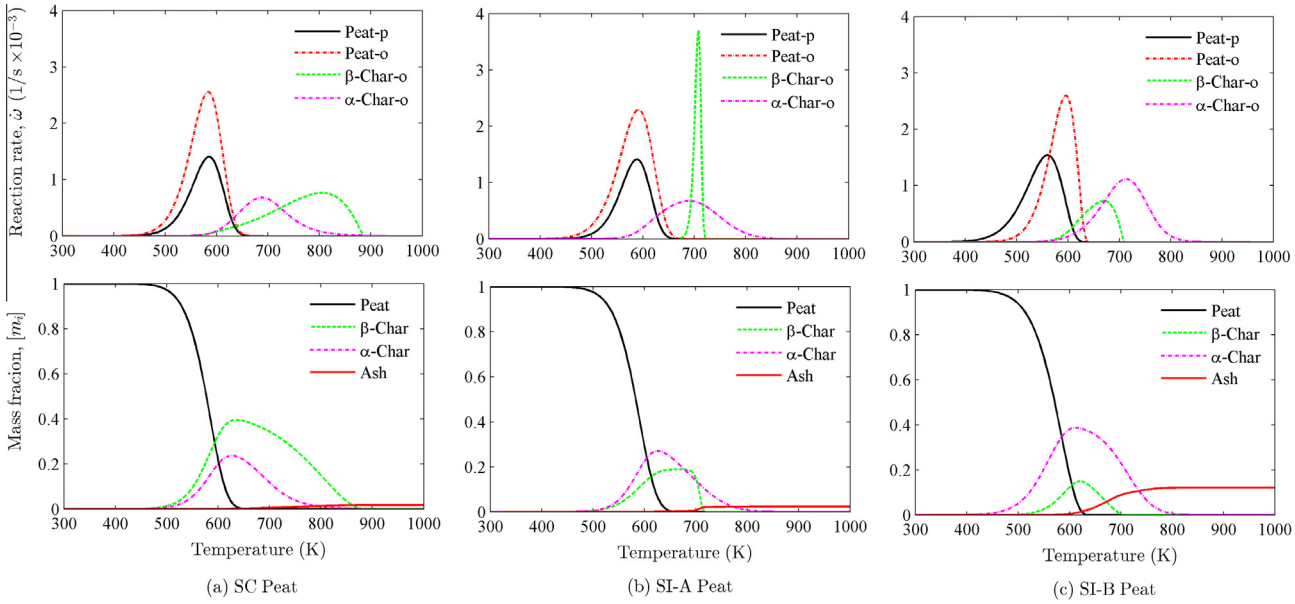

Fig. 9. Modelled reaction rates, $\dot{\omega}_k$ (top) and species mass fraction, m_i (bottom) for (a) SC, (b) SI-A, and (c) SI-B samples in air ($k = 20$ K/min).

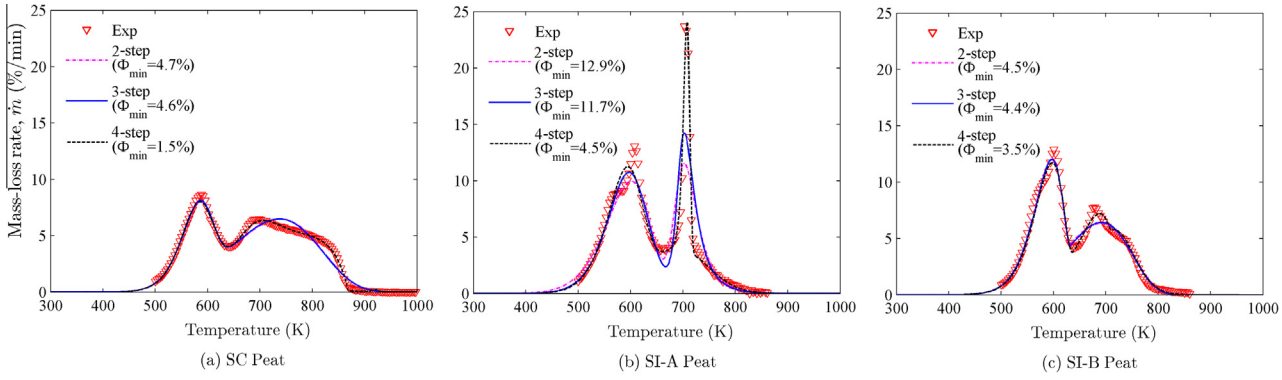

Fig. 10. Mass-loss rate of (a) SC, (b) SI-A, and (c) SI-B peat in air (20 K/min) simulated by kinetics with different steps.

Therefore, including two kinds of char (α-char and β-char) could be crucial to explain the smouldering combustion of peat with a high OC.

4. Application of the kinetics to smouldering front

4.1. 1-D steady-state plug flow model

In this section, a 1-D species plug-flow model is used to explore the different chemical schemes and kinetic parameters, and study the reaction-zone structure of a smouldering front. The spread of a smouldering peat fire has two leading fronts that are significantly different (see Fig. 1: lateral and in-depth spreads). At the in-depth spread, a forward propagation configuration is assumed [3,12], where the airflow by diffusion or convection and the smouldering front moves in the same direction. Both spread modes have been illustrated in more detailed Fig. 11 including the sub-fronts and their orders according to the literature [3,21].

This plug flow model only solves species-conservation equations and is formulated as a boundary-value problem [9]. It assumes a constant smouldering spread rate and a thermal equilibrium between gas and solid phases. Also, it does not solve the energy conservation but uses a prescribed temperature profile instead, converting the original PDE system into an ODE system.

At the lateral spread (Fig. 11a), smoulder spreads along the top soil surface with an abundant oxygen supply, implying that the oxygen depletion in the reaction zone is negligible. So only species conservation for solid species is considered:

$$\frac{dm_i}{d\xi} = -Da_s \sum_k \nu_{i,k}\dot{\theta}_k, \tag{17}$$

where ξ is the non-dimensional spatial variable along the propagation direction (*i.e.* along the top surface) with respect to the characteristic smoulder-front thickness L; and the Damköhler number in solid phase is defined as $Da_s = (L/S)/\tau$. According to Eq. (6), the non-dimensional reaction rate is scaled by a characteristic time τ as

$$\dot{\theta}_k = \tau\dot{\omega}_k = \tau(m_{i,\Sigma})A_k e^{-E_k/RT}\left(\frac{m_i}{m_{i,\Sigma}}\right)^{n_k} Y_{O_2}^{n_{O_2,k}} \tag{18}$$

with $\dot{\theta}_k < 0$ for consumption and $\dot{\theta}_k > 0$ for generation. The density in solid phase, ρ_s, is assumed to be constant and same for all species. Eq. (17) in the lateral spread (1-D in space) is equivalent to Eq. (8) in the TGA (1-D in temperature), but their heating rates are different.

The boundary conditions for Eq. (17) are related to the species mass fractions ahead of the front (see in Fig. 11a), specified as

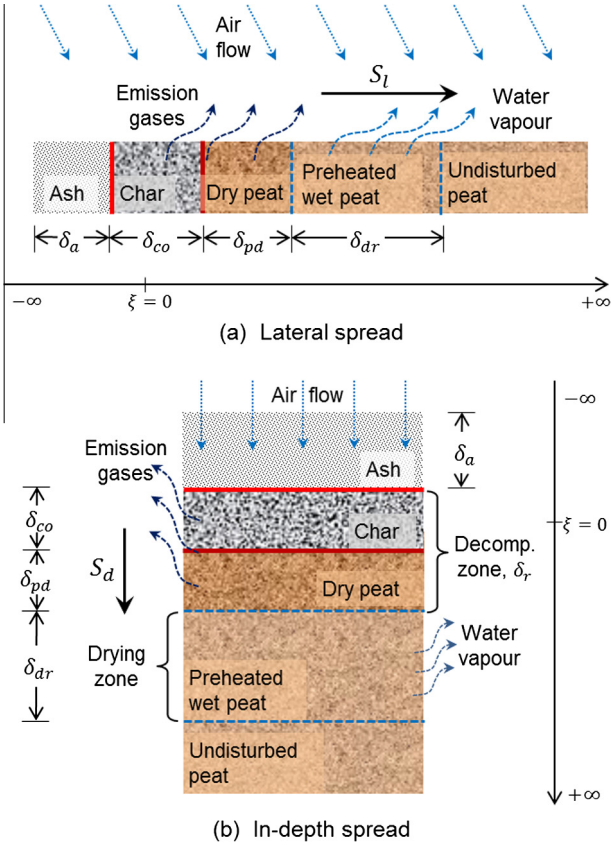

Fig. 11. Spread modes of 1-D smouldering combustion: (a) lateral spread; and (b) in-depth spread. See Fig. 1 for a combined illustration of these fronts.

$$\begin{cases} m_w(\xi = +\infty) = m_{w,0}, \\ m_p(\xi = +\infty) = 1 - m_{w,0}, \\ m_c(\xi = +\infty) = m_\beta(\xi = +\infty) = m_a(\xi = +\infty) = 0. \end{cases} \tag{19}$$

The non-dimensional temperature profile is prescribed as

$$\Pi = \frac{T - T_\infty}{T_s - T_\infty} = \begin{cases} 1, & \xi \leqslant 0 \\ \exp(-\eta\xi), & \xi > 0 \end{cases} \tag{20}$$

where T_s is the peak smouldering temperature, and $\eta = SL/\alpha_s$ is estimated from non-dimensional analysis of the Fourier's law with the upstream solid-phase thermal diffusivity, α_s. That is, the temperature profile is steeper for a larger spread rate.

At the in-depth spread (Fig. 11b), smoulder spreads into the deep soil layers with a limited oxygen supply, so the oxygen conservation is also solved and coupled with solid species in heterogeneous reactions. By invoking mass conservation in the plug-flow model with a constant inlet airflow velocity, u_g, the mass fraction of oxygen in the gas phase varies as

$$\frac{dY_{O_2}}{d\xi} = -\frac{\rho_s}{\rho_g} Da_g \sum_k \nu_{O_2,k}\dot{\theta}_k. \quad (21)$$

At $\xi = -\infty$, we assume

$$Y_{O_2}(\xi = -\infty) = y_{O_2,a}, \quad (22)$$

where ξ is along the direction of in-depth spread; the Damköhler number in gas phase is defined as $Da_g = L/(u_g - S)/\tau$; and the gas density, ρ_g, varies as the ideal-gas law. The inlet oxygen first diffuses through the ash layer before reaching the reaction zone, so an oxygen concentration lower than the atmospheric value is selected for $Y_{O_2,-\infty}$. A steady-state propagation is achieved when oxygen is completely consumed in the reaction zone. The temperature profile is also defined by Eq. (20). All parameters used in the model are summarized in Table 4. Note that the characteristic time, τ, is set to scale the non-dimensional reaction rates in the order of 1.

4.2. Results of lateral spread

The shallow-front spread is first modelled with the proposed 5-step kinetics (drying plus 4 decomposition reactions) and the corresponding kinetics parameters. For the sake of space limitations, only the results of CH and SC samples are reported. The drying parameters of the SC sample are assumed to be the same as that of the CH sample in Table 2.

Figure 12 shows the reaction rates and mass fractions at the lateral spread. These are qualitatively similar to those in Figs. 5 and 9a, as expected from the similarity between Eqs. (8) and (17). Three very distinct propagating sub-fronts are observed: drying, peat decomposition, and then followed by char oxidation, agreeing with experimental observations in [12,21]. In particular, the role of the drying front is captured here for the first time. The thickness of each propagating sub-front is found when the non-dimensional reaction rate is dominant with a threshold value of 0.01: $\delta_{dr}/\delta_{pd}/\delta_{co}$ is 2.7/0.6/0.8 cm (CH sample), and 2.6/0.9/0.8 cm (SC sample). Similar relative positions are also observed for SI-A and SI-B samples, but not repeated here. The information is clear: the drying front is long, and if moisture content increases, the drying front will become longer, so as to slower or forbid the fire spread.

For the CH sample (Fig. 12a) the peat-pyrolysis zone is longer than the peat-oxidation zone ($\delta_{pp}/\delta_{po} \approx 2$). But peat pyrolysis is much slower than peat oxidation ($\dot{\omega}_{po}^{max}/\dot{\omega}_{pp}^{max} = 21$), and the majority of the original peat (90%) is oxidized. Consequently, the β-char oxidation dominates at high temperature. For the SC sample (Fig. 12b), both of the parallel paths (a and b) are important, but peat oxidation is still larger than pyrolysis ($\dot{\omega}_{po}^{max}/\dot{\omega}_{pp}^{max} = 2$), and up to 65% of peat is oxidized. In summary, at the lateral spread, peat oxidation and the corresponding reaction path of (Peat→β-char→ash) are more important.

The validity and accuracy of the reaction-zone structure at the lateral spread is expected to be high because its environment is similar to that of the TG experiment in air, which can be viewed as a good reproduction of larger scales. For this reason, it is expected if a reduced kinetics can well explain the TG experiment in air, it can accurately capture the reaction-zone structure of the lateral spread. Figure 12 also shows the reaction-zone structure modelled from 3-step decomposition scheme plus drying, Eqs. (15) and (1). The comparison with the original 4-step decomposition scheme reveals a small difference because a close degree of fit is found in Figs. 7 and 10.

Table 4
Parameters used in plug flow model.

Parameter	Value	Unit	References/notes
MC	50%	kg/kg	–
$\nu_{O_2,po}$	0.3	–	[12,39]
$\nu_{O_2,co}$	1.0	–	[12,39]
ρ_s	150	kg/m^3	[12]
α_s	10^{-7}	m^2/s	[40]
L	1	cm	Scaling
τ	600	s	Scaling (=10 min)
T_s	800	K	[21,41]
S_l	0.50	mm/min	[41]
S_d	0.29/0.26	mm/min	CH/SC peat (cal.)
u_g	0.80	mm/s	Dimensional analysis
$Y_{O_2,a}$	0.12	–	Assumed

4.3. Results of in-depth spread

The same 5-step kinetics is applied to CH and SC samples at the in-depth spread. The oxygen stoichiometric coefficients for oxidations of peat ($\nu_{O_2,po}$), α-char ($\nu_{O_2,\alpha o}$), and β-char ($\nu_{O_2,\beta o}$) are obtained from carbon emission measurements [39], and assumed to be proportional to the heat of oxidation [9]. The heat of reaction can be estimated from the elemental composition [12,14,15], and assumed to be proportional to the mass loss of organic content in each step. The oxygen diffusion velocity is estimated from the dimensional analysis of Fick's law, $u_g \sim \sqrt{\alpha_g/\tau}$ where the gas thermal diffusivity α_g is in the same order of molecular diffusivity. Figure 13 shows the reaction rates and species distribution for in-depth spread.

The calculated in-depth spread rate is reported in Table 4, in the same order (~0.1 mm/min) of experimental observations [3,41]. In general, the oxidation rate as well as the in-depth spread rate is lower than that of lateral spread because of the oxygen depletion. For the CH sample (Fig. 13a), a similar three-propagation-front structure is observed, but the dimension becomes larger where $\delta_{dr}/\delta_{pd}/\delta_{co}$ follows 3.6/1.5/1.1 cm. Compared to the lateral spread, the peat-decomposition zone is larger, but the peat-oxidation zone inside becomes even thinner ($\delta_{pp}/\delta_{po} = 10$). Thus, larger fraction of the original peat (36%) is pyrolyzed (only 10% at the lateral spread), and the oxidation rates of the two chars are comparable at high temperature. For the SC sample (Fig. 13b), the propagation fronts also become larger: $\delta_{dr}/\delta_{pd}/\delta_{co}$ follows 4.0/1.9/1.0 cm. Pyrolysis becomes dominant, 98% of the peat is pyrolyzed, and so as the α-char oxidation at high temperature. In short, at the in-depth front the pyrolysis and the corresponding path of (peat → α-char →ash) becomes more important or even dominant because the oxygen supply is limited upstream.

The validity and accuracy of reduced decomposition schemes (3-step and 2-step) plus drying are also explored in Fig. 13. For the CH sample, 3-step scheme, Eq. (15) including pyrolysis, gives a good agreement. Meanwhile, although 2-step scheme, Eq. (16), can give a good degree of fit to the TG curve in Fig. 7, the result for in-depth spread is misleading, where the peat-decomposition zone becomes very thin and overlapping with the char-oxidation zone. The major reason is that the 2-step scheme does not include the oxygen-independent pyrolysis. Thus, it cannot capture the oxygen-limited character of in-depth spread.

Now, focus on the SC sample in Fig. 13b, although the reduced 3-step scheme gives a similar peat-decomposition zone, the thickness of char-oxidation zone becomes doubled and the char oxidation becomes much mild. For the 2-step scheme, similar misleading results are shown: the peat-decomposition zone becomes thinner and partially overlapping with the high-temperature

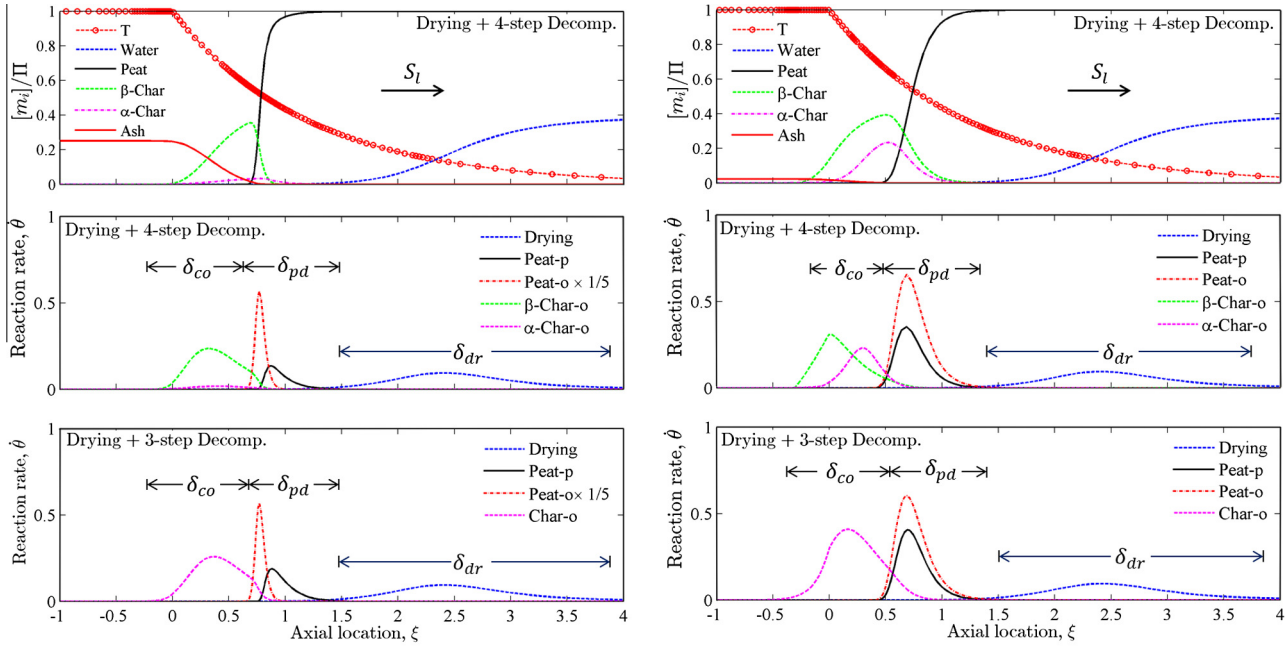

(a) CH Peat at shallow front (lateral spread) (b) SC Peat at shallow front (lateral spread)

Fig. 12. Reaction-zone structure of the lateral spread for (a) the CH peat; and (b) the SC peat.

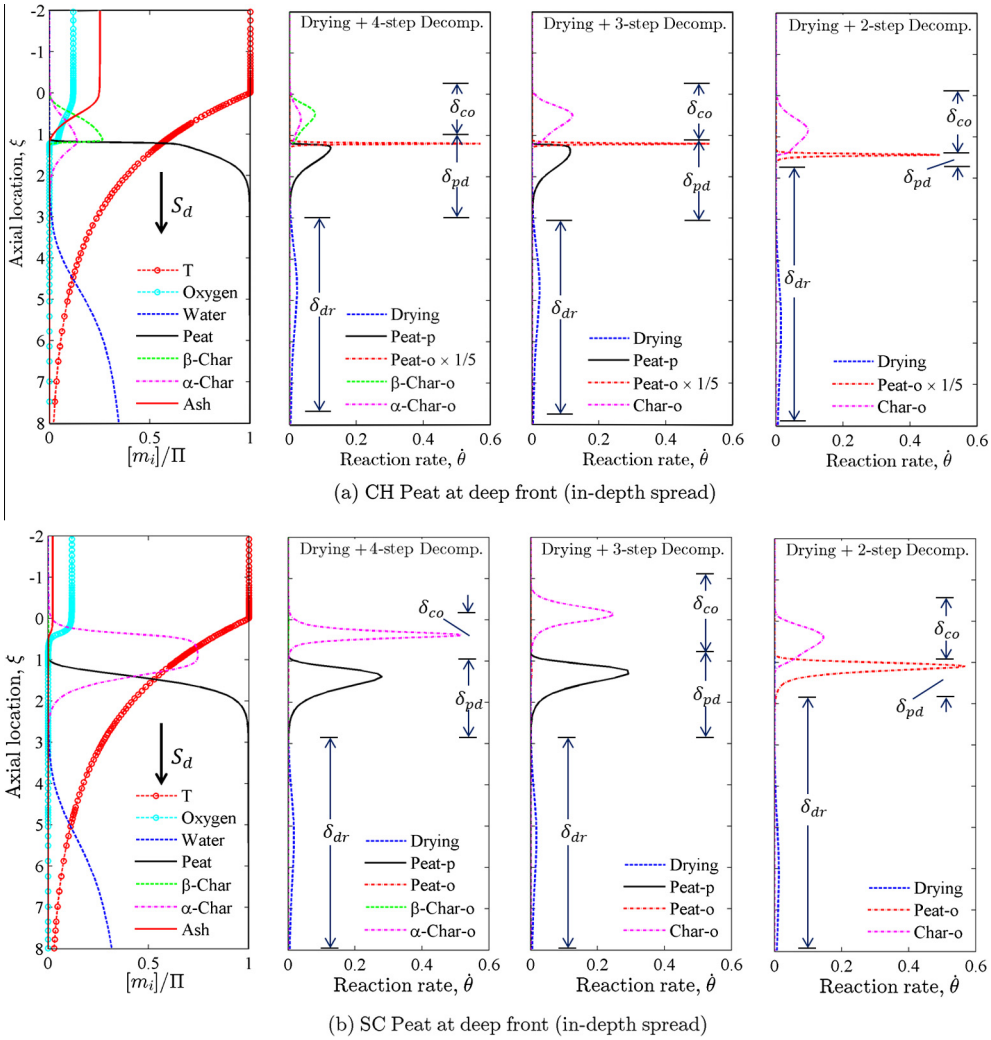

(a) CH Peat at deep front (in-depth spread)

(b) SC Peat at deep front (in-depth spread)

Fig. 13. Reaction-zone structure of the in-depth spread for (a) the CH peat, and (b) the SC Peat.

char-oxidation zone, although in Fig. 10a these step-reduced schemes can give a comparable degree of fit as the 4-step decomposition. In summary, a kinetic scheme, having good agreement with TG experiments, is not necessarily beneficial for more accurately modelling smouldering combustion under various environmental conditions, unless it includes all the important dominant physics. In order to further improve the model accuracy, TG testing under various oxygen concentrations is necessary.

5. Conclusions

In this work, a 5-step kinetics (1-step drying and 4-step decomposition) is proposed for smouldering combustion of peat. The scheme includes one pyrolysis, and three oxidations, plus 1-step drying with 5 condensed species (water, peat, α-char, β-char, and ash). The corresponding inverse problem on TG data is solved to find the best kinetic and stoichiometric parameters for four types of boreal peat. Reduced 3-step and 2-step decomposition schemes are found to give reasonable agreements with TG data as well. The results show that at the TG level, all proposed schemes seem to perform well, with a high degree of agreement resulting from the forced optimization in the inverse problem approach.

The chemical validity of the schemes is then investigated outside the TG realm and incorporated into a 1-D plug-flow model to study reaction and the species distribution inside a peat smouldering front. Both lateral and in-depth spread modes are considered. The results show that the drying sub-front is essential, and the best kinetics is the 4-step decomposition. At the lateral spread, the structure is found to be similar to that in the TG experiment because of the analogy between time in TG and space in a 1-D moving framework. The path of (peat $\rightarrow\beta$-char $\rightarrow$ash) is dominant. At the in-depth spread, modelling results show that the oxygen consumption controls the thickness of the reaction front. Moreover, the pyrolysis as well as the path of (peat$\rightarrow\alpha$-char$\rightarrow$ash) becomes more important in the in-depth mode. It is also found that the reduced kinetic scheme without pyrolysis (2-step) give misleading predictions of in-depth spread, despite the apparent agreement with TG data.

This is the first time that the smouldering kinetics and the reaction-zone structure of a peat fire are explained and predicted, thus helping to understand this important natural and widespread phenomenon. Future work will focus on the initiation and spread of smouldering peat fires with a comprehensive multiphysics model, including heat, mass, and momentum transport in the porous bed.

Acknowledgments

X. Huang is supported by the Exceptional Overseas Scholarship from the Department of Mechanical Engineering at Imperial College London and G. Rein is supported by EPSRC. The authors thank Haixiang Chen (University of Science and Technology of China) and Valérie Leroy-Cancellieri (University of Corsica) for providing the TG data.

References

[1] T. Ohlemiller, Progress in Energy and Combustion Science 11 (1985) 277–310.
[2] D. Drysdale, An Introduction to Fire Dynamics, Wiley, 2011.
[3] G. Rein, in: C. Belcher (Ed.), Fire Phenomena and the Earth System, Wiley and Sons, 2013, pp. 15–33, http://dx.doi.org/10.1002/9781118529539.ch2.
[4] S.E. Page, F. Siegert, J.O. Rieley, H.-D. V. Boehm, A. Jaya, S. Limin, Nature 420 (2002) 61–65.
[5] G.M. Davies, A. Gray, G. Rein, C.J. Legg, Forest Ecol. Manag. 308 (2013) 169–177.
[6] B. Poulter, J. Christensen, L. Norman, P.N. Halpin, J. Geophys. Res. 111 (2006).
[7] L. Moreno, M.-E. Jimenez, H. Aguilera, P. Jimenez, A. Losa, Fire Technol. 47 (2011) 519–538.
[8] C.D. Blasi, Prog. Energy Combust. Sci. 34 (2008) 47–90.
[9] G. Rein, C. Lautenberger, A.C. Fernandez-Pello, J.L. Torero, D.L. Urban, Combust. Flame 146 (2006) 95–108.
[10] S. Vyazovkin, C.A. Wight, Annu. Rev. Phys. Chem. 48 (1997) 125–149. PMID: pmid:15012442.
[11] J.A. Gonzlez-Prez, F.J. Gonzlez-Vila, G. Almendros, H. Knicker, Environ. Int. 30 (2004) 855–870.
[12] R.M. Hadden, G. Rein, C.M. Belcher, Proc. Combust. Inst. 34 (2013) 2547–2553.
[13] T. Kashiwagi, H. Nambu, Combust. Flame 88 (1992) 345–368.
[14] D. Cancellieri, V. Leroy-Cancellieri, E. Leoni, A. Simeoni, lexander Ya. Kuzin, lexander I. Filkov, G. Rein, Fuel 93 (2012) 479–485.
[15] H. Chen, W. Zhao, N. Liu, Energy Fuels 25 (2011) 797–803.
[16] W.H. Frandsen, Can. J. Forest Res. 17 (1987) 1540–1544.
[17] W.H. Frandsen, Can. J. Forest Res. 27 (1997) 1471–1477.
[18] H. Grumpelt, in: F. Ullmann (Ed.), Ullmann's Encyclopedia of Industrial Chemistry, Wiley-VCH, 2000.
[19] J. Koppejan, S. van van Loo, The Handbook of Biomass Combustion and Co-firing, Taylor & Francis, 2012.
[20] J. Brandrup, E. Immergut, E. Grulke, Polymer Handbook, Polymer Handbook Series, John Wiley & Sons, 1999.
[21] G. Rein, N. Cleaver, C. Ashton, P. Pironi, J.L. Torero, Catena 74 (2008) 304–309.
[22] M. Pansu, J. Gautheyrou, Handbook of Soil Analysis: Mineralogical, Organic and Inorganic Methods, Springer, 2006.
[23] E. Plaster, Soil Science and Management, Texas Science Series, Delmar Cengage Learning, 2008.
[24] A. Chammari, B. Naon, F. Cherblanc, B. Cousin, J.C. Bnet, Drying Technol. 26 (2008) 836–843.
[25] A.I. Filkov, A.Y. Kuzin, O.V. Sharypov, V. Leroy-Cancellieri, D. Cancellieri, E. Leoni, A. Simeoni, G. Rein, Energy Fuels 26 (2012) 349–356.
[26] F. He, F. Behrendt, Combust. Flame 158 (2011) 2500–2511.
[27] M. Amutio, G. Lopez, R. Aguado, M. Artetxe, J. Bilbao, M. Olazar, Fuel 95 (2012) 305–311.
[28] C. Lautenberger, C. Fernandez-Pello, Fire Safety J. 44 (2009) 819–839.
[29] J.A. Foster, Nat. Rev. Genet. 2 (2001) 428–436.
[30] J. Arora, Introduction to Optimum Design, Elsevier Science, 2004.
[31] S.L. Kokjohn, R.M. Hanson, D.A. Splitter, R.D. Reitz, Int. J. Engine Res. 12 (2011) 209–226.
[32] T.-Y. Park, G.F. Froment, Comput. Chem. Eng. 22 (1998) S103–S110. European Symposium on Computer Aided Process Engineering-8.
[33] L. Elliott, D. Ingham, A. Kyne, N. Mera, M. Pourkashanian, C. Wilson, Prog. Energy Combust. Sci. 30 (2004) 297–328.
[34] C. Lautenberger, G. Rein, C. Fernandez-Pello, Fire Safety J. 41 (2006) 204–214.
[35] C. Houck, J. Joines, M. Kay, GAOT: A Genetic Algorithm for Function Optimization: A Matlab Implementation, Technical Report, Report NCSU-IE TR 95-09, 1995. <http://www.ie.ncsu.edu>.
[36] A. Lesnikovich, S. Levchik, J. Therm. Anal. 30 (1985) 677–702.
[37] D.M. Marquis, E. Guillaume, A. Camillo, T. Rogaume, F. Richard, Combust. Flame 160 (2013) 818–829.
[38] R. M. Hadden, Smouldering and Self-Sustaining Reactions in Solids: An Experimental Approach, Ph.D. thesis, University of Edinburgh, 2011. <http://hdl.handle.net/1842/3528>.
[39] G. Rein, S. Cohen, A. Simeoni, Proc. Combust. Inst. 32 (2009) 2489–2496.
[40] Y. Viswanadham, N. Jagan Mohana Rao, Pure Appl. Geophys. 101 (1972) 247–260.
[41] N. Prat, Personal communication, Unpublished experimental data, 2013.